JTTEE5 16:168–176
DOI: 10.1007/s11666-007-9037-4
1059-9630/$19.00 © ASM International

Commentary

Quantifying Thermal Spray Coating Architecture by Stereological Protocols: Part II. Key Points to be Addressed

Guy Antou and Ghislain Montavon

(Submitted January 21, 2007)

This commentary aims at presenting, from a practical viewpoint, some key points to assess when implementing image analysis coupled to stereological protocols to quantify statistically the architecture of thermal spray coatings and their relevant features (pores, lamellae, and so forth.). This article is the second of a two-part commentary; the first one, published in *Journal of Thermal Spray Technology*, Vol 16 (No. 1), 2007, detailed those stereological protocols from a historical perspective.

Keywords image analysis, image capture, polishing protocol, stereology, structural quantification

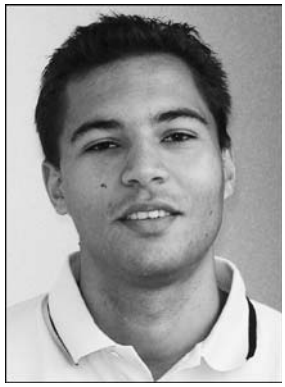

Guy Antou

Ghislain Montavon

1. Implementing Stereology on Thermal Spray Coatings

Thermal spray coatings exhibit fairly complex architecture, which results from the stacking of individual lamellae formed by consecutive impact, spreading, and solidification of impinging molten or semimolten particles during several passes of the spray torch. These lamellae can be of various composition (for example, a mixture of several oxides) and nature (for example, composite coatings such as cermets). Several features constitute the structure of thermal spray coating:

- Lamellae, called the matrix
- Spherical particles corresponding either to particles unmolten during their flight due to improper trajectories, or to the core of partially molten particles (usually, the biggest ones of a given particle size distribution), or particles that resolidified before their impact onto the substrate (usually, the smallest ones of a given particle size distribution) or, finally, too small particles that recirculate into the surrounding atmosphere due to turbulent dispersion
- In the case of metallic coatings sprayed at atmosphere, globular oxides embedded within the lamellae and formed during the particle flight and interlamellar oxides formed during and after the lamellae formed prior to the impact at the same location of further particles
- Globular pores (i.e., cavities) corresponding either to stacking defects or to pores embedded within particles at their impact
- Delaminations corresponding to interlamellar decohesion consecutive, for example, to vapors and gases stagnating in the vicinity of the surface to be coated and peripheral decohesions around lamellae
- Cracks corresponding to intralamellar cracks that develop consecutively to the particle rapid solidification process after spreading (such a phenomenon is especially emphasized for ceramic materials, which do not comply very much with the thermal contraction after solidification)
- Core-shaped pores associated with large unmolten particles and usually located at the base of those particles, resulting from a shadow effect

Thermal spray layers exhibit an orthotropic architecture caused by their deposition mechanism; that is, they

Guy Antou, SPCTS—UMR CNRS 6638, Ecole Nationale Supérieure de Céramiques Industrielles, 47-73 Avenue Albert Thomas, 87065, Limoges Cedex, France; **Ghislain Montavon,** SPCTS—UMR CNRS 6638, Faculty of Sciences, University of Limoges, 123 Avenue Albert Thomas, 87060, Limoges Cedex, France. Contact e-mail: guy.antou@unilim.fr.

have two orthogonal planes of symmetry (i.e., following the spray direction and perpendicular to the spray direction). Orthotropy contrasts with isotropy (i.e., no particular directionality within the structure) and anisotropy (i.e., directionally dependent following the three directions of space).

In this case, and since metallographic analyses are usually accomplished on cross sections because of the opacity of the microstructures, attention is drawn to the fact that an observation following a cross-sectioned plane does not necessarily reflect the entire three-dimensional microstructure, but only the intersection of the structure with this specific plane. A body cut following three different orthogonal test planes may exhibit three different architectures. In such conditions, results deduced from such observations have to be analyzed with respect to an appropriate perception.

As illustrated in Fig. 1, the implementation of stereological protocols leading to the quantitative interpretation of the coating architecture constitutes the ultimate step of a long procedure that comprises successively (1) sample preparation (sampling, mounting, prepolishing and polishing, and eventually etching), (2) image acquisition, (3) image pretreatment, (4) image treatment, and finally (5) stereology implementation.

The reader may think that such a long procedure may be too tedious. In fact, the steps related to image pretreatments and treatments can be very easily automated as can be the implementation of stereology. This means that implementing stereology does not require too significant an effort compared with qualitative analysis of coating architecture. Indeed, the two first steps are necessary in both cases.

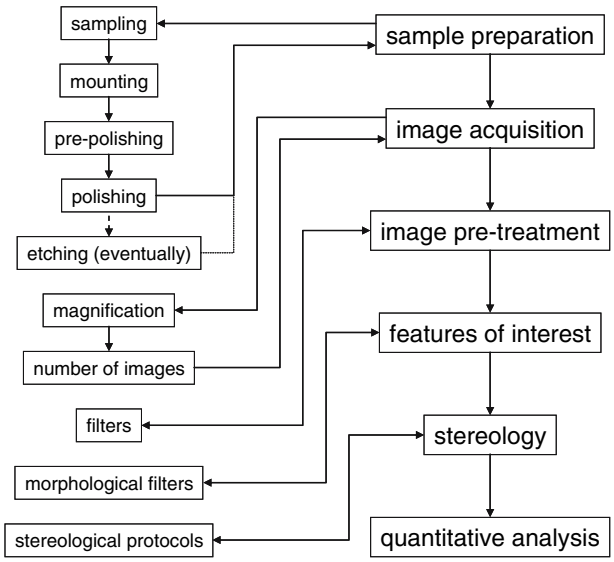

Fig. 1 Steps to be implemented to carry out stereological analyses

2. Basic Rules for Image Acquisition

2.1 Metallographic Preparation

Metallographic preparation is *the* key point to be addressed when implementing stereological protocols since sample preparation can significantly damage the structures to be analyzed. Some readers will say that whatever the quality of the preparation, it will damage the structure one way or another. However, appropriate protocols can significantly limit damage or generate ''reproducible'' damage, permitting at least comparison of the stereological data between different samples.

Sample preparation consists of up to five consecutive steps, namely cutting, mounting, prepolishing, polishing, and, in some cases, etching.

Cutting aims to produce a planar surface of a representative sample. This is done by abrasive cutting using either resinous or metallic matrix saws. The nature (i.e., ''hardness'') of the saw has to be adapted to the nature of the coating to be cut, the ''harder'' the coating, the ''softer'' the saw, and inversely. ISO 150525-1975E standard specifies the nomenclature of abrasive saws.

During abrasive cutting, about 70% of the energy is converted into heat, which can be transmitted to the sample. For comparison, only about 5% of the energy is converted into heat during conventional machining. In such a case, damages can result from abrasive cutting, especially decohesion within the structure. This is why the cutting speed, the transverse speed, and the lubricant have to be properly defined. Commonly:

- Cutting speed should be on the order of a few hundred meters per minute.
- Transverse speed should vary between 0.01 and 0.1 mm/s. It is suggested, when possible, to select the lowest possible transverse speed and to use a device in which the cutting speed can be adjusted rather than the cutting load, since in this latter case the cutting speed varies along the sample.
- Water or oil have to be used as lubricant.

Samples have to be mounted in such a way that the cutting pressure is applied to the substrate to limit delaminations at the coating/substrate interface as much as possible. Samples are usually fixed in a dedicated vise, and protection (encapsulation) of the sample surfaces by soft materials (such as a polymer film) is recommended to limit the stress concentration in case of improper alignment or rough coating surface and hence to prevent the coating from cracking.

To summarize, applying the following motto is recommended: better spend more time for cutting the sample; this will result in reduced polishing time and in less damage to the structure.

The main goal of the mounting process is to manufacture a sample that can be easily manipulated and to reinforce the coating prior to polishing. Several techniques can be implemented, usually typified as ''cold'' and ''warm'' mounting, using thermosetting and thermoplastic

resins, respectively. From the author's experience, ''warm'' mounting should be avoided as the relatively high pressure and high temperature required for mounting the samples irremediably damage them. In the case of ceramic coatings, this mounting method often leads to delamination and spallation during polishing. In the case of metallic coatings, it leads to a ''softening'' of the coating caused by the thermal treatment encountered by the sample during mounting and by possible delamination at the coating/substrate interface following stress relaxation. ''Cold'' mounting can be performed using epoxy, acrylic, or polyesters resins. The selection of the resin is governed by identifying a compromise between the curing duration, the resin viscosity, and the shrinking during curing. The optimal resin has low viscosity and low shrinking. This implies in turn a relatively long curing duration (up to 12 h in some cases). Epoxy resins are preferred as they correspond to these characteristics.

Most of the time, when considering porous coatings, it is also recommended to perform this step under reduced pressure to get a good impregnation of the pore network by the resin. This technique is known as ''vacuum impregnation.''

It is possible to add some additives to the resin, conferring to it specific characteristics such as an electric conductivity for scanning electron microscopy (SEM) observation (this does not replace the application of sputtered gold or carbon layer onto the polished surface prior observation), a higher hardness limiting the differential wear at the sample edges during polishing, or a different color. It is also possible to add fluorescent additives permitting the highlighting, when observed by optical microscopy with an appropriate ultraviolet light, of very thin defects within the structure. When implementing image analysis coupled to stereological protocols, fluorescent additives have to be absolutely avoided as the fluorescence leads systematically to an overestimation of the size of the features.

The prepolishing step should result in a planar sample surface with low amount of damage and deformation and consists of submitting the mounted sample to abrasion machining using either silicon carbide (the most encountered solution) or alumina papers or lapping disks. Silicon carbide papers should not be used for more than 3 min; they can damage the structure since the machining process can change from abrasion (with abrasive particles fixed onto their paper support) to grinding (abrasive particles roll between the paper support and the sample).

If the cutting step has been performed following appropriate rules, it is possible to limit the prepolishing step to a few paper grades only and to begin the operation at a relatively high grade, that is, P600 at least.

The polishing step is intended for obtaining a mirror finish of the sample surface, that is, a surface with singularities of a very low amplitude, usually on the order of one-tenth of a micrometer. Polishing is done usually with diamond, colloidal silica, or alumina as abrasive particles, depending mostly on the nature (i.e., mechanical and chemical properties) of the coating to be polished. These particles are either embedded or dispersed onto polishing clothes of various textures and mechanical characteristics. A careful selection of the nature of the polishing clothes has to be made depending on the nature of the coating to be polished.

The same recommendations apply to both prepolishing and polishing steps, in particular:

- Use semi- or automatic polishing machine for a higher reproducibility of the operation.
- Adjust independently the load on each sample to polish a given coating nature at the appropriate pressure regardless of the sample size.
- Select identical directions of rotation for the samples and the abrasive support to avoid damage by spallation.

The Thermal Spray Society Committee on Accepted Practices has published recently in this Journal a series of articles on the best practices for sectioning (Ref 1), mounting (Ref 2), grinding (Ref 3), and polishing (Ref 4) thermal spray coatings. The reader is referred to these articles for more details about sample preparation.

2.2 Image Acquisition

Capture of images by SEM rather than by optical microscopy (OM) is recommended because the higher resolution of SEM images usually leads to better results. During image acquisition, the parameters of the SEM must be controlled. The acquisition mode (i.e., the secondary electron [SE] mode or the backscattered electron [BSE] mode) has to be chosen to obtain a sharp contrast between the studied features (for example, different phases or the matrix and the pore network), which renders more efficient the later segmentation of the images for analysis. The SE mode generally makes it possible to achieve higher resolution (of about a few nanometers in the best cases). The resolution reached by the BSE mode is lower than the one reached by the SE mode. The SE mode resolution depends on the interaction between the influx electrons and the material, thus on the SEM operating parameters (voltage and electronic current) and on the material nature. However, images of smooth surface (such as polished surface) exhibit generally low contrast. The BSE mode, which is sensitive to the average atomic number of the sample, gives a high contrast between dissimilar phases. Moreover, the annular geometry of the BSE detector, centered at the midpoint of the influx electron impact point, induces no shadowing effect.

The parameters of the column have to be fixed and maintained constant for all images of a same study: the voltage, the working distance, and the spot size have an effect on the gray-level distribution of the image. The brightness and the contrast must be selected and optimized: the brightness induces a shift of the gray-level distribution toward lower or higher values, whereas a decrease of the contrast reduces the gray-level span and can cause a loss of information.

Moreover, the architectures are usually heterogeneous and can be characterized at several scales. Consequently,

the size of the representative elementary volume (REV) must be defined to describe the overall structure of the material. The REV size is often defined by the magnification of the microscope images, because the image resolution is given by a fixed number of pixels on the charge-coupled device (CCD) camera. On the one hand, the REV must be small enough to resolve the thinner details of the structure (such as microcracks): this requires a high magnification and a high image resolution. On the other hand, the REV must be large enough to describe the whole material structure that requires a low magnification. Consequently, a compromise must be found between a high resolution and a low magnification to define a REV, *which has to be representative of the structure independently of its location within the sample.*

In order to determine the number of images that must be measured to obtain a statistically significant result, the evolution of the result variability (standard deviation over average value) must be followed as a function of the considered number of images (Fig. 2). The appropriate number of images corresponds to the value where this function tends toward an asymptote.

2.3 Image Pretreatment

Several mathematical filters can be implemented to reveal specific structural data from the initial image (Ref 5). The objective of this pretreatment is to remove singularities and to reveal feature outlines prior to morphological analysis. It consists of altering the pixel values (i.e., pixel intensities) using mathematical treatments.

Four main types of filters are usually implemented at this stage of the treatment:

- Filters that make it possible to modify the image contrast (linear or nonlinear filters)
- Arithmetic and logic filters
- Spatial filters (linear or nonlinear filters)
- Frequency filters (Fast Fourier Transform, FFT, applicable only on square images)

2.3.1 Contrast Modification. A contrast modification consists of altering the pixel initial values to modify the contrast and/or the brightness. The modifications of the pixel intensities are given by a transfer function, which can be linear or nonlinear, continuous or discontinuous.

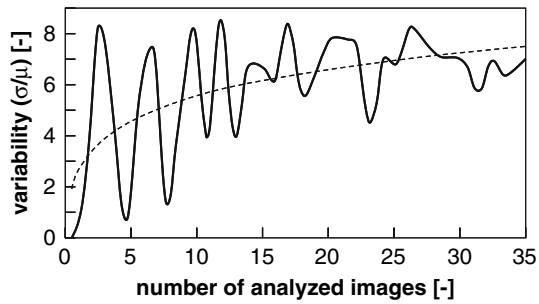

Fig. 2 Determination of the number of images to be analyzed

Table 1 summarizes the main functions commonly used to alter the contrast and/or brightness. The equalization filter is quasi-systematically implemented as it performs a linear expansion of the gray-level histogram. It makes it possible hence to avoid gray-level losses by covering the whole visualization field (Fig. 3).

2.3.2 Arithmetic and Logic Filters. The arithmetic and logic filters alter pixel intensities independently of the neighbor pixel intensities. Consequently, the image resulting from the transformation originates directly from pixel intensities that have the same coordinates in the initial image.

Table 2 summarizes the main logic and arithmetic filters that are commonly implemented. It can be noticed that these filters are largely used to compare several images or to define analysis masks, which permit selection of specific areas.

2.3.3 Spatial Filters. Spatial filters modify the intensity of each pixel as a function of the intensities of neighbor pixels. They are mainly employed to detect boundaries or outlines of studied features, to reduce the background noise of the image, or to underline some singularities.

There are two types of spatial filters: (a) high-pass filter that detects the elevated variations of pixel intensities (i.e., to visualize of the object outlines) and (b) low-pass filter

Table 1 Main functions used to alter the contrast and/or brightness

Function	Definition	Effect
Equalization	Average on a given gray-level range	Increase the brightness and the contrast
Potency	$f' = f^{1/Y}$	Increase the brightness and the contrast in the darkest domains
Square root	$f' = \sqrt{f}$	
Logarithmic	$f' = \ln f$	
Potency	$f' = f^{Y}$	Reduce the brightness and the contrast in the lightest domains
Square	$f' = f^{2}$	
Exponential	$f' = \exp f$	

f' = altered pixel intensity after transformation; f = initial pixel intensity.

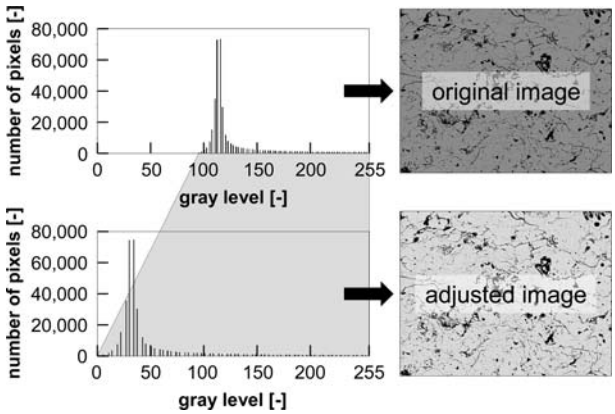

Fig. 3 Linear expansion of the gray-level histogram by the equalization filter

Table 2 Main logic and arithmetic filters

Type of operation	Operation
Arithmetic filters	Multiply
	Divide
	Add
	Subtract
Logic filters	AND
	OR
	XOR

Table 3 Main spatial filters

Filter	High-pass	Low-pass
Linear	Gradient	Smoothing
	Laplace	Gauss
Nonlinear	Gradient	Median
	Roberts	Low-pass
	Sobel	N order
	Prewitt	...
	Sigma	...

that smoothes the variations of pixel intensities (i.e., to weaken the image details). The modification of the pixel intensity is made using a linear or nonlinear combination of the neighbor pixel intensities. The neighbor pixels of the analyzed pixel are localized by a square matrix, or a mask, of $n \times n$ dimension (for example, 3×3, 5×5, etc.). The value of the analyzed pixel intensity is modified by a combination of the $n \times n$ matrix pixel intensities. Table 3 displays some examples of spatial filters.

These filters must be carefully implemented because they induce a modification of the information embedded in the image. For instance, the median filter can be used to eliminate a pulsed noise on an image captured by optical or scanning electron microscopy (Fig. 4). However, the use of this filter modifies the image information by the loss of the thinner objects (i.e., the microcracks).

2.3.4 Frequency Filters. The frequency filters give a new representation of the image in the frequency space. The spatial frequency corresponds to the fluctuation of the illuminated intensities according to the spatial coordinates. It is based on the signal theory: a signal is the sum of sinusoids resulting from several frequencies. A real image is a superposition of two-dimensional sinusoids. One image of one two-dimensional sinusoid will correspond to a point in the frequency space. The Fourier transformation of a function $g(u, v)$ $(u, v = 0 \ldots n)$, which represents a square image, is:

$$G(x,y) = \sum_{u=0}^{n} \sum_{v=0}^{n} g(u,v) \times e^{-2\pi i(ux+vy)/n} \quad \text{(Eq 1)}$$

These filters are used to: (a) characterize a signal (for example, in electronic microscopy, it makes it possible to reveal a spatial frequency in the gray-level distribution), (b) detect and rebuild a periodic signal that exhibits noises (for instance, in crystallography, it makes it possible to reveal atomic rows on a high-resolution image captured by transmission electron microscopy, Fig. 5), (c) filter and deconvolute periodic noise on an image, and (d) perform autocorrelation and cross-correlation.

3. Identification of Features of Interest by Image Analysis

3.1 Segmentation

Detection of objects to be analyzed is possible by image segmentation. Segmentation consists of defining two regions on the image: a region corresponding to the digital objects set to an intensity value of 1, and the background set to an intensity value of 0.

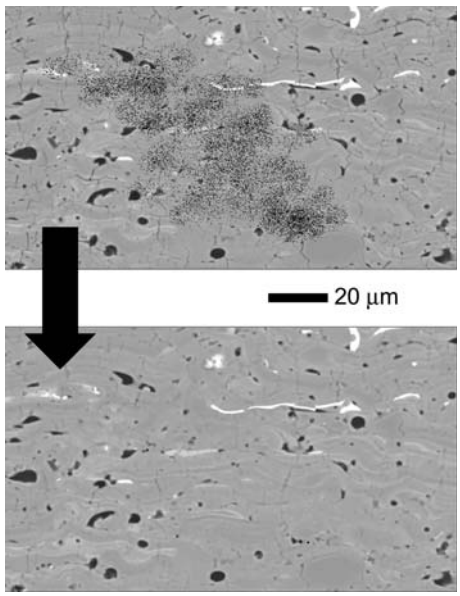

Fig. 4 Implementation of the median filter to suppress a pulsed noise on a scanning electron microscopy image (cross section of a gray alumina coating manufactured by air plasma spraying; gray features: alumina; white features: titania; dark features: pores)

Two methods exist to generate a binary image: the threshold method and the density slice method (Fig. 6). The selection of the method depends on the studied structure. However, the density slice method offers more potential.

The threshold level is not randomly chosen. It is calculated by analyzing the gray-level distribution and by determining the value that optimizes the separation between the different objects (Fig. 7).

3.2 Morphological Analysis

Morphological filters can be employed to suppress the artifacts in the binary image or to isolate some objects (Ref 5). Four primary filters are commonly used:

- The "erosion" filter removes pixels from the edges of the objects, where contiguous black areas in the image are considered objects, and background is assumed to be white. A pixel is removed (set to white) if four or more of its eight neighbors (depending on the selected

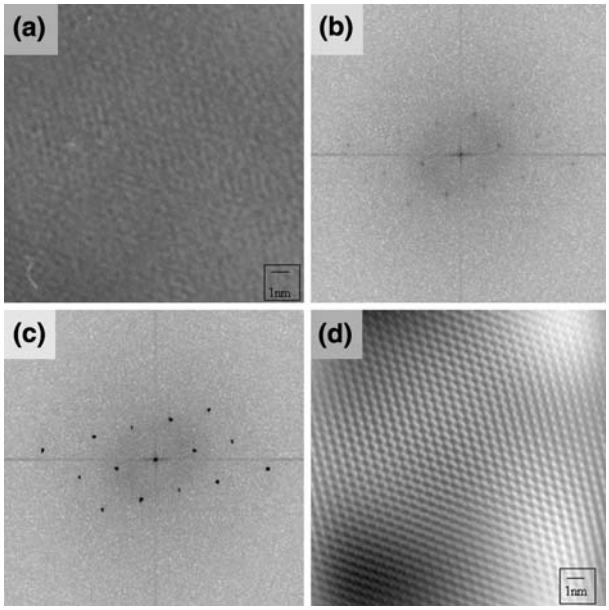

Fig. 5 Visualization of atomic rows on a high-resolution image captured by transmission electron microscopy (http://www.cep.ensmp.fr/scpi/DocMateriel/MET.htm). (a) Original image. (b) Fast Fourier Transform (FFT) of (a). (c) Filtered FFT. (d) Inverse FFT of (c)

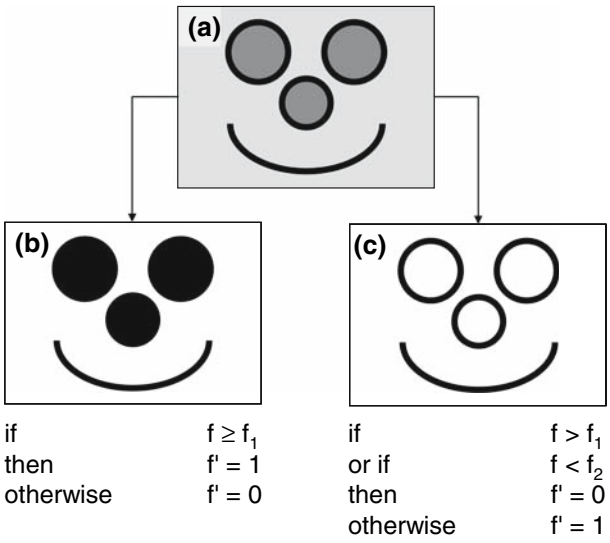

Fig. 6 Segmentation of an image by thresholding or density slicing

option) are white. Erosion separates objects that are touching and removes isolated pixels.

- The ''dilatation'' filter has an opposite effect compared to the ''erosion'' filter. It adds pixels to the edges of the objects. A pixel is added (set to black) if four or more of its eight neighbors (depending on the selected option) are black. Dilatation connects discontinuous objects and fills in holes.

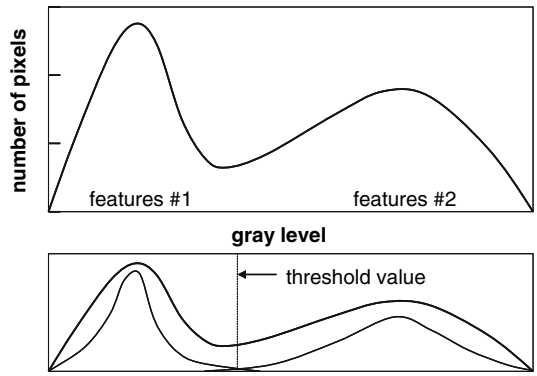

Fig. 7 Calculation of the threshold level for an image that presents two types of features with different gray levels

- The ''open'' filter successively executes the ''erosion'' and ''dilatation'' filters. It smoothes the outlines of the digital objects and removes isolated pixels (Fig. 8).
- The ''close'' filter has an opposite effect compared to the ''open'' filter. It successively executes the ''dilatation'' and ''erosion'' filters. It smoothes the outlines of the digital objects and fills in isolated ''holes'' within objects that correspond most of the time to artifacts.

The digital objects are characterized by their intensity interval. In the case of a binary image, the digital objects are composed of the pixels that exhibit the same intensity (usually, an intensity equal to 1 and a background equal to 0). In the case of gray-level image, the digital objects are defined according to an intensity range. All the pixels that fall into a specific intensity range are put together to form a digital object (usually, one pixel belongs to a digital object if one or more of its neighbors belongs to this object).

When the digital objects are defined and detected, it is then possible to make a morphological analysis by specifying morphological criteria (size and shape factors) and spatial criteria (distribution of the objects in the image plane). Six classes of morphological and spatial criteria can be distinguished (Table 4).

3.3 Examples of Application

Image analysis was carried out on SEM images of gray alumina coatings (Fig. 9a) (Ref 6). Al_2O_3-13TiO_2 coatings were atmospheric plasma sprayed using several sets of power parameters to scan their effects on the pore network architecture. Namely, the arc current intensity (ranging from 350 to 700 A), the plasma gas composition (hydrogen to argon ratio, ranging from 10 to 33%), and the plasma gas total flow rate (ranging from 40 to 70 SLPM) were considered. Analysis permitted the identification of (a) the major effects of power parameters on the pore architecture and (b) the related formation mechanisms of those pores.

The samples were cut parallel to the spray direction using a resinous diamond saw in an oil medium, mounted

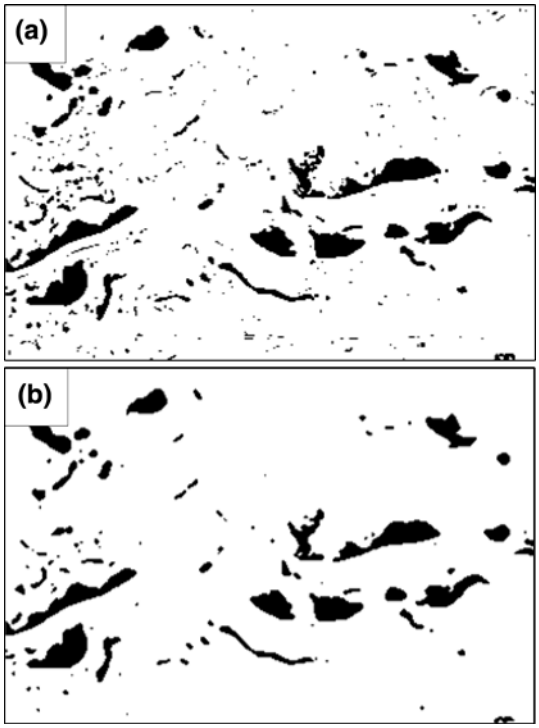

Fig. 8 Example of a morphological treatment using the ''open'' filter on a binary image

Table 4 Main morphological and spatial criteria characterizing a digital object

Class	Criteria
Size	
Area	Object area
	Total analyzed area
	Average level of the object intensity
	etc.
Length	Object perimeter
	Greater length
	Smaller length
	etc.
Equivalent shape	Minor axis of the equivalent ellipse(a)
	Major axis of the equivalent ellipse
	Length of the equivalent rectangle(b)
	Width of the equivalent rectangle
	etc.
Localization	Mass center according to x and y
	Maximal coordinates according to x and y
	Minimal coordinates according to x and y
	etc.
Orientation	Object orientations according to x and y
	Greater length orientation
	Object projection according to x and y
	etc.

(a) Equivalent ellipse: ellipse with the same area and the same orientation than the digital object. (b) Equivalent rectangle: rectangle that is contained or contains the digital object.

in rings and infiltrated under low pressure with epoxy. They were then polished following standard metallographic techniques (i.e., prepolishing and diamond slurry polishing) on an automatic polishing system (Table 5). Prior to SEM observation, a carbon layer was deposited by sputtering onto the polished samples. The chosen magnification was 1100×, which results in an image resolution of 0.31 μm per pixel and a selected area of 152×224 μm^2. The defined REV corresponds to the whole coating thickness, which makes it possible to take into account the possible heterogeneity throughout the coating thickness.

Table 5 Polishing protocol for the gray alumina coatings

Step	Paper grade or particle average size	Polishing plate velocity, rpm	Specimen carrier velocity, rpm	Load, N	Time, min
1	SiC grade P600	150	60	17	3
2	SiC grade P1200	150	···	···	3
3	Diamond 9 μm	200	···	···	10
4	Diamond 3 μm	200	···	···	15
5	Diamond 1 μm	200	···	···	15
6	Diamond 0.1 μm	150	···	···	10

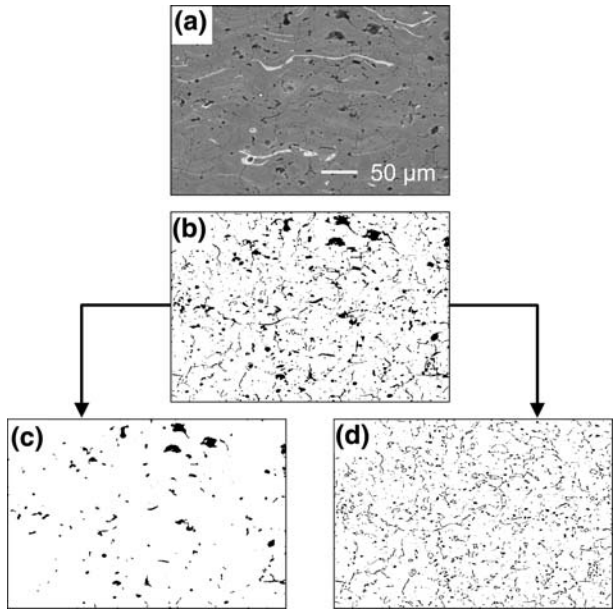

Fig. 9 Image analysis for discriminating the globular pores from the crack network

Scanning electron images were analyzed using Scion Image Alpha 4.0.3.2. software (Scion Corporation, 82 Worman's Mill Court, Suite H, Frederick, MD), which is based on NIH Image for Macintosh Operating System (National Institutes of Health, USA). First, image analysis permitted the quantification of the overall porosity level and the crack network orientation (i.e., the Delesse's protocol). Pores and cracks were isolated implementing several filtering and morphological protocols (Fig. 9 and Table 6). Pores were then analyzed in terms of numbers and relative surfaces, and cracks in terms of cumulated lengths and orientations. Interlamellar (perpendicular to spray direction) and intralamellar (parallel to spray direction) cracks were discriminated and analyzed

Table 6 Main filters used to isolate pores and cracks for the gray alumina coatings

Step	Purpose	Implemented tools	Corresponding figure
1	Image segmentation	Threshold function	Fig. 9(b)
2	Globular pore isolation	Erosion and dilatation filters; arithmetic and logic filters (OR)	Fig. 9(c)
3	Crack network restitution	Arithmetic and logic filters (XOR)	Fig. 9(d)

Table 7 Crack pore network characteristics by Delesse's analysis and corresponding in-flight particle and particle spreading characteristics vs. operating parameters

In-flight particle characteristics		Particle spreading characteristics						Coating pore network characteristics					
V, m/s	*T*, °C	ρ, kg/m^3	μ, Pa/s	ν, N/m	Re(a)	We(b)	*K*	Total, %	σ(c), %	Globular, %	σ(c), %	Crack, %	σ(c), %
256	2,324	2,890	0.047	0.63	600	15,377	614	6.3	0.3	1.5	0.1	4.8	0.2
226	2,157	2,908	0.068	0.69	370	8,357	401	7.3	0.3	2.1	0.1	5.1	0.1
282	2,458	2,875	0.036	0.59	845	23,801	832	5.8	0.2	1.2	0.1	4.5	0.1
216	2,196	2,904	0.062	0.67	385	8,307	404	6.3	0.5	1.8	0.2	4.6	0.3
275	2,384	2,883	0.042	0.62	721	19,824	730	7.3	0.3	1.9	0.2	5.3	0.1
245	2,304	2,892	0.049	0.64	551	13,502	563	8.6	0.4	3.3	0.3	5.3	0.1
269	2,347	2,887	0.045	0.63	658	17,695	674	5.3	0.3	1.1	0.1	4.2	0.1

(a) Reynolds number. (b) Weber number. (c) σ = standard deviation associated to the average value. Source: Ref 2.

separately. The cumulated length of cracks per unit surface, L_A (m^{-1}), was calculated to deduce the cumulated surface of cracks per unit volume, A_V (m^{-1}), according to the following stereological relationship: (Ref 7)

$$A_V = \frac{4}{\pi} L_A \quad \text{(Eq 2)}$$

In addition, the DeHoff's protocol for ellipsoidal particles (Ref 8, 9), derived from the Schwartz-Saltykov's analysis (Ref 10) for spherical particles, permitted the analysis of the pore size distribution (i.e., repartition of the pore relative volume in each size class). Each pore in the plane of observation is considered to be an ellipse of major axis (M), minor axis (m), and axial ratio ($q = m/M$). Pores in volume are then modeled as ellipsoids of revolution by rotation of the ellipses around their minor axis (i.e., oblate ellipsoids). Pores were then divided into 15 size classes. The increment of size class, Δ, was equal to $M_{max}/15$ where M_{max} is the highest ellipse major axis in the largest size class.

For each size class (Δ_i), the equivalent ellipsoidal volume (V_i) and the number of ellipsoidal particles per volume unit (N_{V_i}) were determined as:

$$V\bar{i} = \frac{\pi}{6} \cdot (M_{\max i})^3 \cdot \bar{q}i \quad \text{(Eq 3)}$$

$$N_{V_i} = \frac{(N_A)_i}{\overline{M_i \cdot k_i}} \quad \text{(Eq 4)}$$

where $M_{max\ i}$ is the maximum major axis for the considered size class, $\overline{q_i}$ is the average axial ratio, $(N_A)_i$ is the number of pores per image area, $\overline{M_i}$ is the average major axis, and $\overline{k_i}$ is the average DeHoff's shape factor. The DeHoff's shape factor (k) for oblate ellipsoids is defined as:

$$k(q) = \int_0^{\frac{\pi}{2}} \int_0^{\frac{\pi}{2}} \frac{\sqrt{1 + (q^2 - 1) \cdot \cos^2 \varphi}}{\pi/2} \cdot \sin \varphi \cdot d\varphi \cdot d\theta \quad \text{(Eq 5)}$$

where q represents the average ellipse elongation ratio.

It is hence possible to calculate the porosity relative volume (V_{V_i}) for each size class:

$$V_{V_i} = V_i \cdot N_{V_i} \quad \text{(Eq 6)}$$

For each processing parameter set, the results were averaged from 15 fields of view randomly selected across the corresponding polished cross section.

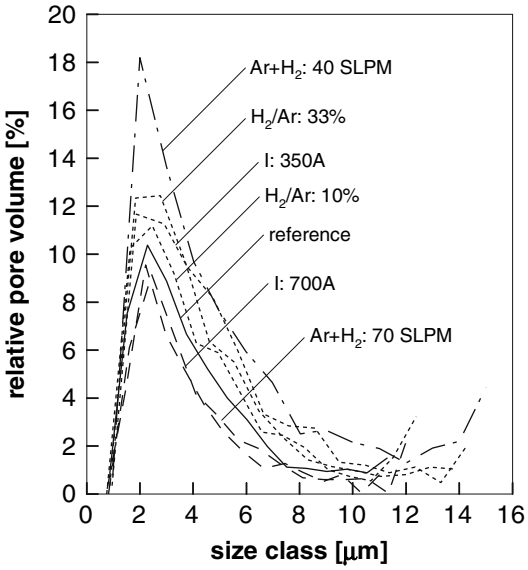

Fig. 10 Pore size distribution by DeHoff's analysis. Source Ref 2

The porosity level, the repartition and the linear density of cracks have been quantified using Delesse's protocol (Table 7). The DeHoff's protocol permits the quantification of the pore size distributions (Fig. 10) that are bimodal in a first approximation. It is implicitly considered in this case that the spatial distribution of pores within the structure is almost isotropic (i.e., isotropic approximation). This was confirmed by analyzing the average free path between pores. These results are correlated to the corresponding in-flight particle and particle spreading characteristics. It suggests relationships between the in-flight particle characteristics (Reynolds, Weber, and Sommerfeld numbers, and particle temperature) and the resulting porous architecture. It finally makes it possible to study the mechanisms leading to the formation of pore features.

4. Concluding Remarks

Stereological protocols, of the first or the second order, aim at statistically quantifying three-dimensional structures from two-dimensional—randomly oriented—plane sections, in terms of size-shape and spatial distributions, respectively.

The implementation of stereological protocols constitutes the ultimate step of a long procedure including successively (1) sample preparation (sampling, mounting, prepolishing and polishing, and eventually etching), (2) image acquisition, (3) image pretreatment, (4) image treatment, and finally (5) stereology implementation.

Sample preparation is the *key* step in this procedure since inappropriate preparation protocols may damage the structure to be quantified consecutively to the generation of scratches, pull-outs, delaminations, and so forth.

Concerning image acquisition, the representative elementary volume (REV) has to be defined depending on the characteristics (size and spatial distribution) of the features of interest to be analyzed. Improper REV selection may introduce biases or require too many images to be captured.

Several filters make it possible to pretreat the images to highlight the features of interest prior to binarization, and morphological filters are used to suppress artifacts from binary images. Several protocols based on the measurement of areas on plane sections can be then selected to analyze the architecture of thermal spray coatings.

Several quantitative tools allowing the quantification of complex structures exist. They are known as stereological protocols. These are widely used in as various fields as biology, neurology, botany, astronomy, earth observation, metallurgy, and materials science, among others. They have also proven to be applicable to the quantification of some specific features of thermal spray coatings, and we encourage the reader to implement some of them as they appear to us as powerful tools to quantify the architecture of thermal spray coatings.

References

1. J.P. Sauer, Metallographic Preparation and Testing of Thermal Spray Coatings: Sectioning, TSS Committee on Accepted Practices, *J. Thermal Spray Technol.*, 2005, **14**(3), p 313-314
2. D.G. Puerta, Metallographic Preparation and Evaluation of Thermal Spray Coatings: Mounting, TSS Committee on Accepted Practices, *J. Thermal Spray Technol.*, 2005, **14**(4), p 450-452
3. D.G. Puerta, Metallographic Preparation and Testing of Thermal Spray Coatings: Grinding, TSS Committee on Accepted Practices, *J. Thermal Spray Technol.*, 2006, **15**(1), p 31-32
4. J.P. Sauer and G. Blann, Metallographic Preparation and Testing of Thermal Spray Coatings: Fine Grinding & Polishing, TSS Committee on Accepted Practices, *J. Thermal Spray Technol.*, 2006, **15**(2), p 174-176
5. J.C. Russ, The Image Processing Handbook, (2nd ed.)., CRC Press, Inc, Boca Raton, FL, 1995
6. G. Antou, G. Montavon, F. Hlawka, A. Cornet, and C. Coddet, Exploring Thermal Spray Grey Alumina Coating Pore Network Architecture by Combining Stereological Protocols and Impedance Electrochemical Spectroscopy. *International Thermal Spray Conference 2006* (Seattle, WA), 2006, May
7. E.E. Underwood, Stereology, or the Quantitative Evaluation of Microstructures, *J. Microscopy*, 1969, **89**(2), p 161-180
8. R.T. DeHoff and F.N. Rhines, Determination of Number of Particles per Unit Volume from Measurements Made on Random Plane Sections: The General Cylinder and the Ellipsoid, *Trans. Metall. Soc. AIME*, 1961, **221**, p 975-982
9. R.T. DeHoff, The Determination of the Size Distribution of Ellipsoidal Particles from Measurements Made on Random Plane Sections, *Trans. Metall. Soc. AIME*, 1962, **224**, p 474-477
10. S.A. Saltykov, The Determination of the Size Distribution of Particles in an Opaque Material from a Measurement of the Size Distribution of their Sections. *Stereology*, H. Elias, Ed., Springer-Verlag, New York City, 1967, p 163-173